J. Magn. Soc. Japan, 24, 1367–1373 (2000) 〈Contributed Paper〉

Interface Effects on Magnetic and Magneto-Optical Properties in TbFeCo/Pt Multilayers

Yusuke Itoh,[1] William Van Drent,[2] Masahiro Birukawa,[3]
Katsuaki Sato* and Takao Suzuki
Information Storage Materials Laboratory, Toyota Technological Institute,
2-12-1 Hisakata, Tempaku-ku, Nagoya 468-8511
*Faculty of Technology, Tokyo University of Agriculture and Technology,
2-24-16 Nakacho, Koganei, Tokyo 184-8588

The present paper discusses the effect of Pt on the magnetic and magneto-optical properties in TbFeCo/Pt multilayer films fabricated by sputter-deposition, in conjunction with interfacial structures. Both the magnetic and magneto-optical properties as a function of Pt thickness are reasonably well explained on the basis of a model in which an interfacial region very similar to an Fe–Pt alloy is assumed. Furthermore, low angle X-ray diffraction analysis and polar Kerr magneto-optical spectra simulation over a photon energy range from 1.4 to 6.8 eV (wavelength $\lambda=182$ to 886 nm) reveal that the Fe–Pt alloy-like interfacial regions are formed only on top of TbFeCo layers, but not on Pt layers. A possible contribution of polarized Pt atoms to the magneto-optical spectra is also discussed.

Key words: multilayer, interfacial alloy, magneto-optical Kerr effect, polarized Pt, amorphous TbFeCo alloy

1. Introduction

Platinum atoms are known to be effective for the enhancement of the magneto-optical effect at short wavelengths at around 400 nm in Co/Pt multilayers.[1)–4)] It was also elucidated that Pt can be used to improve read-out characteristics at short wavelengths in combination with the conventional rare-earth transition-metal (RE-TM) material.[5)] Previous work[6),7)] discussed the effect of Pt additives as spacers in TbFeCo/Pt multilayer structure on both magnetic and magneto-optical properties. It was then suggested that Fe–Pt alloy-like interfacial regions, which are formed through interdiffusion between TbFeCo and Pt layers, enhance both the net magnetization and polar Kerr activity at ultraviolet photon energies.[8)–11)] In order to elucidate this mechanism, the present paper discusses detailed interfacial structures based on low angle X-ray diffraction and polar Kerr magneto-optical spectra.

2. Experimental

Multilayer films of $Tb_{23}Fe_{69}Co_8$/Pt were fabricated by sputter-deposition in Ar atmosphere. The base pressure prior to deposition was better than 5×10^{-8} Torr. The Ar gas pressure was 5 mTorr during deposition. Films were deposited onto glass substrates. The layer-thicknesses of TbFeCo (t_{TbFeCo}) and Pt (t_{Pt}) were varied over a range of 10–100 Å and 0.5–30 Å, respectively. The composition of the amorphous TbFeCo layer was determined by electron probe microanalyzer and was kept constant for all the multilayers under consideration. Multilayer films of two different types were prepared: (i) 500–550 Å thick multilayers with a 30 Å thick Pt-overcoat, purposed for measurements of magnetic properties, and (ii) 250–300 Å thick multilayers fabricated onto a 750 Å thick Pt reflective layer without overcoating for optical measurements. Measurements of magnetic properties were carried out using a vibrating sample magnetometer and a torque magnetometer in fields up to 15 kOe. The magneto-optical polar Kerr spectra and the optical constants were measured from the sample surface side, immediately after deposition using a Kerr spectrometer for photon energies ranging between 1.4 and 6.8 eV (wavelength $\lambda=182$–886 nm).[12),13)] Low angle X-ray diffraction measurements were carried out with Cu-$K_{\alpha1}$ radiation at 50 kV/300 mA.

3. Results

3.1 Structural analyses

Figure 1 shows a high resolution cross-sectional TEM photograph of a 5× {TbFeCo 30 Å/Pt 24 Å} multilayer observed at 200 keV accelerating voltage. The dark and light contrasts correspond to those of Pt and TbFeCo layers, respectively. Though one can not ascertain about the interfacial structure in this TEM picture, the overall layered structure is well established.

Low angle X-ray diffraction patterns for different Pt thicknesses in {TbFeCo 30 Å/Pt t Å} multilayers, with $t=3$, 12, and 30 Å are given in Fig. 2. A well-defined periodic structure is observed in these patterns. The main peaks marked with $n=1, 2, \cdots$ correspond to the

Present address: [1]Material Engineering Div. III, Toyota Motor Corporation, *1200 Mishuku, Susono, Shizuoka 410-1193*; [2]ADE Technologies, Inc., *77 Rowe Street, Newton, Massachusetts 02466, U.S.A.*; [3]Optical Disk Systems Development Center, Matsushita Electric Industrial Co., Ltd., *1006 Kadoma, Kadomashi, Osaka 571-8501.*

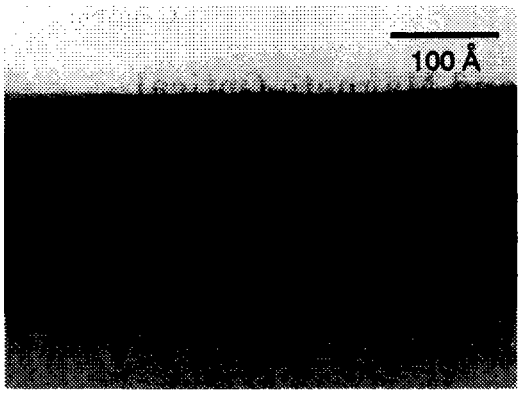

Fig. 1 Cross-sectional TEM photograph of a 5× {TbFeCo 30 Å/Pt 24 Å} multilayer+30 Å SiN_x overcoat.

first, second, ··· order diffraction from the (TbFeCo/Pt) bilayers. The actual bilayer thicknesses Λ_{meas} determined from the positions of these bilayer peaks are presented in Table 1. These Λ_{meas} values are found to be in reasonable agreement with the designed values (Λ_{des}) but are all smaller by about 10%. This reduction may possibly be attributed to the open/close processes of shutters during deposition, while the sputter-deposition rate was calibrated based on the continuously integral total deposition. The small oscillation seen in these profiles reflects the interference effect due to the total film thickness (~500 Å).

3.2 Magnetic properties

A sequence of polar Kerr hysteresis loops for Pt thicknesses (t_{Pt}=0, 1, 3, 6, and 12 Å) in {TbFeCo 30 Å/Pt} multilayer films is presented in Fig. 3. These loops were measured at λ=830 nm at room temperature. The polarity reversal of the loop can be observed between (a) t_{Pt}=0 (TbFeCo single layer film) and (b) t_{Pt}=1 Å, indicating an occurrence of the magnetic-structural change from the RE-rich to TM-rich characteristics. The coercivity decreases as t_{Pt} increases and the hysteresis loop becomes distorted for t_{Pt} larger than 3 Å.

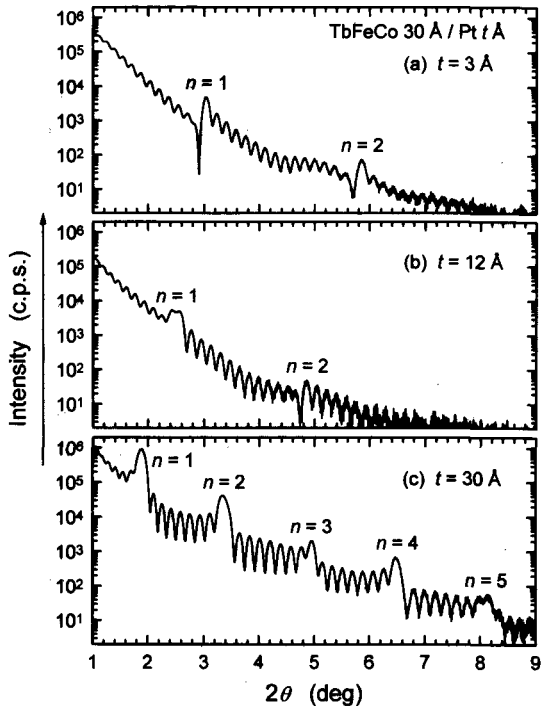

Fig. 2 Low angle X-ray diffraction patterns of TbFeCo/Pt multilayers. (a) 15× {TbFeCo 30 Å/Pt 3 Å}, (b) 12× {TbFeCo 30 Å/Pt 12 Å}, and (c) 8× {TbFeCo 30 Å/Pt 30 Å}.

Figure 4(a) shows the coercivity H_c at room temperature as a function of Pt thickness for two different thicknesses of TbFeCo, *i.e.*, t_{TbFeCo}=30 and 50 Å. For small t_{Pt} values, the H_c increases rapidly with t_{Pt} up to 1 Å, implying the so called compensation point is close to 1 Å. This is also supported by the polarity reversal of the polar Kerr loop occurring at around t_{Pt}=1 Å. Therefore, the subnetwork magnetization of TM(Fe, Co) apparently becomes predominant over that of RE(Tb) as t_{Pt} increases. For larger t_{Pt} values, the H_c decreases rapidly with t_{Pt} up to 10 Å.

The intrinsic perpendicular magnetic anisotropy con-

Table 1 Bilayer thickness and fitting result for low angle X-ray diffraction data

Multilayer	Designed bilayer thickness Λ_{des} (Å)	Measured bilayer thickness Λ_{meas} (Å)	Model	Thickness fitting result (Å) Stacking direction → Pt	FePt	TbFeCo	FePt	Fitting reliability R' (%)
TbFeCo 30 Å / Pt 3 Å	33	31						
TbFeCo 30 Å / Pt 12 Å	42	37	*Symmetric*	8	5.6	19	5.6	9.6
			Asymmetric (1)	4	0	23	11.2	6.9
			(2) *Reversed*	1	11.2	25	0	8.6
			(3) *Roughness*	1	(σ_j= 11 Å)	26	11.2	2.4
TbFeCo 30 Å / Pt 30 Å	60	55	*Symmetric*	22	5.1	22	5.1	7.9
			Asymmetric (1)	25	0	20	10.2	3.7
			(2) *Reversed*	18	10.2	26	0	4.9
			(3) *Roughness*	25	(σ_j= 1 Å)	19	10.2	3.5

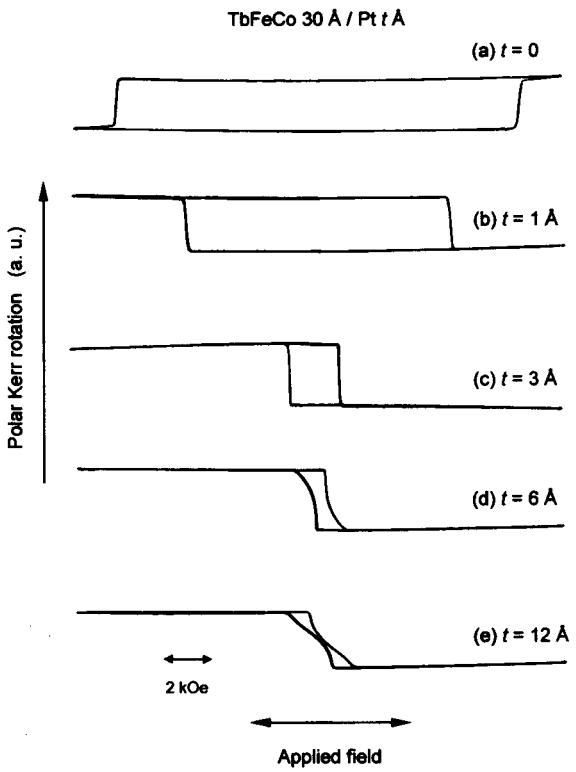

Fig. 3 Polar Kerr hysteresis loops of TbFeCo/Pt multilayers. (a) TbFeCo single layer, (b) 17× {TbFeCo 30 Å/Pt 1 Å}, (c) 16× {TbFeCo 30 Å/Pt 3 Å}, (d) 14× {TbFeCo 30 Å/Pt 6 Å}, and (e) 12× {TbFeCo 30 Å/Pt 12 Å}.

stant K_u was deduced from torque curves measured with external fields up to 15 kOe. Figure 4(b) shows K_u at room temperature as a function of t_{Pt}. It is noted that this K_u is the value per unit volume of the total multilayer. A monotonic decrease of K_u with t_{Pt} is shown for $t_{Pt}>5$Å. For thin Pt regions, the data seems to indicate that the K_u increases with t_{Pt}. However, the field applied in the experiment was insufficient to deduce K_u accurately, and therefore the detailed trend is open to further study.

Figure 4(c) shows the saturation magnetization M_s at room temperature as a function of t_{Pt}. The value of M_s is normalized to the total volume. For both cases, the M_s rises rapidly from the negative value (-44 emu/cm^3, where the negative sign means the RE-rich dominant moment) to the positive value (TM-rich dominant moment) with t_{Pt} up to 12 Å. The dashed line refers to the nominal multilayer calculated assuming that TbFeCo layers solely contribute to the total magnetization, where the slope is determined from the simple dilution by nonmagnetic Pt. It is clearly seen that the actual magnetization behavior is far from this line.

3.3 Magneto-optical spectra

Figure 5 displays the spectra of (a) polar Kerr rotation θ_K and (b) polar Kerr ellipticity η_K for various t_{Pt} in TbFeCo/Pt multilayers with $t_{TbFeCo}=30$ Å. The magneto-optical spectra obtained for a $Tb_{23}Fe_{69}Co_8$ film, which is the same in composition as that of multilayers, are also given in this figure for comparison. As seen in the figure, the peak of θ_K at around 5 eV ($\lambda\sim250$ nm) is enhanced with increasing t_{Pt}. The η_K spectra for the multilayers also exhibit a negative peak at about 5.8 eV. The enhancement in both θ_K and η_K is found to be saturated at $t_{Pt}=12$ Å, which corresponds to the thickness at which the saturation magnetization becomes maximum.

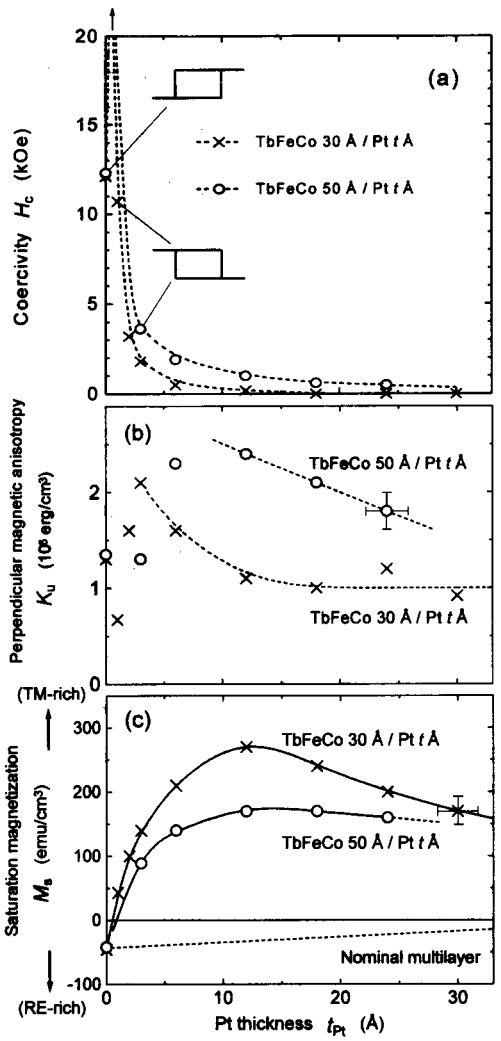

Fig. 4 (a) Coercivity, (b) perpendicular magnetic anisotropy, and (c) saturation magnetization of TbFeCo/Pt multilayers as a function of Pt thickness.

4. Discussion

As shown in Fig. 4(c), the saturation magnetization of TbFeCo/Pt multilayers is strongly enhanced and even changes the sign compared with the calculated values obtained on the basis of the simple dilution. Possible mechanisms for this enhancement may be as follows: 1) Decrease in antiferromagnetically coupled Tb moment due to loss of Tb moment near the interfaces, 2) spin-polarization of Pt close to the interfaces, and 3) formation of interfacial alloy such as Fe–Pt and Co–Pt.

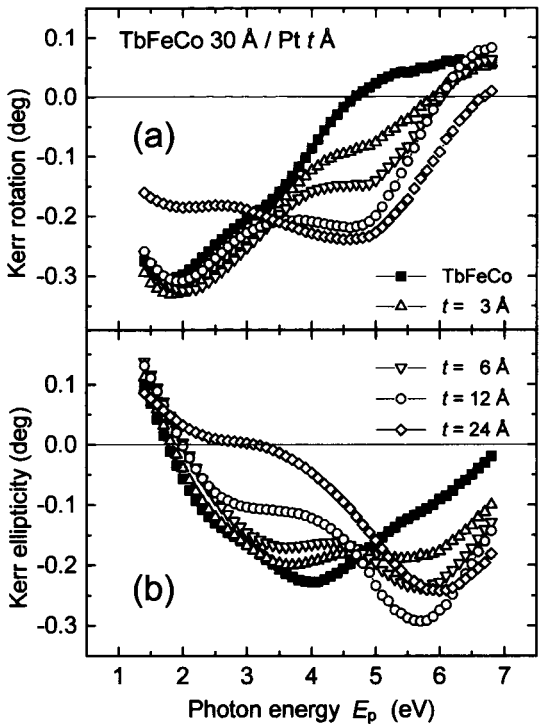

Fig. 5 (a) Polar Kerr rotation and (b) ellipticity for various Pt thicknesses in TbFeCo/Pt multilayers as a function of photon energy.

Induced moment of Pt in Fe matrix has been known to be no more than 0.3 μ_B,[14)-16)] which is too small to account for the enhancement. Therefore, the enhancement is attributed to a formation of interfacial regions. Since the major element in the TbFeCo layer is Fe (69 at%), one would expect the contribution in magnetism and magneto-optical effect from the interfacial regions of Fe-rich composition, while Tb moment has a minor contribution to the total. Therefore, it is reasonable to conjecture that an interfacial region of Fe–Pt alloy-like is formed. The analyses are made in the present study through the model, where the thickness of the interfacial alloy-like is estimated. In this model, one alloy-like layer is assumed for one period since magnetic data can only determine the relative volume of the alloy-like layer. The total magnetization of the multilayer is then expressed by

$$M_{\text{total}}=M_{\text{TbFeCo}}[(t_{\text{TbFeCo}}-\delta/2)/\Lambda] + M_a(\delta/\Lambda)+M_i, \quad (1)$$

where M_{TbFeCo}, M_a, and M_i are the magnetization of TbFeCo, the alloy-like layer, and the induced magnetization in Pt layers, respectively, and δ is the thickness of the alloy-like layer and Λ the bilayer period ($=t_{\text{TbFeCo}}+t_{\text{Pt}}$). Figure 6 shows the δ values estimated using Eq. (1) for different TbFeCo thicknesses ($t_{\text{TbFeCo}}=30$ and 50 Å) as a function of t_{Pt}. In order to explain the observed values of M_s, the M_a value is found to be 1,100 emu/cm^3. This value is comparable to that for the equiatomic composition in Fe–Pt alloy system.[17)] Here, the third term is neglected because the induced moment in

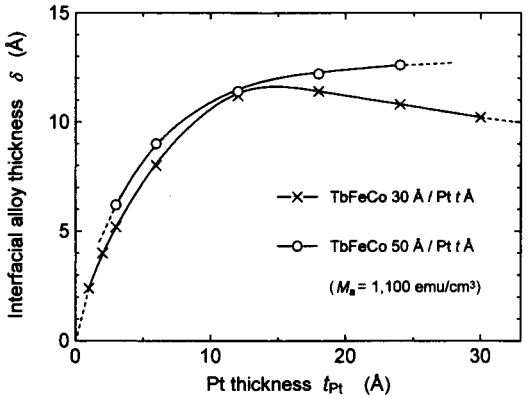

Fig. 6 Plots of interfacial alloy thickness of TbFeCo/Pt multilayers as a function of Pt thickness. These values are estimated provided M_a is 1,100 emu/cm^3.

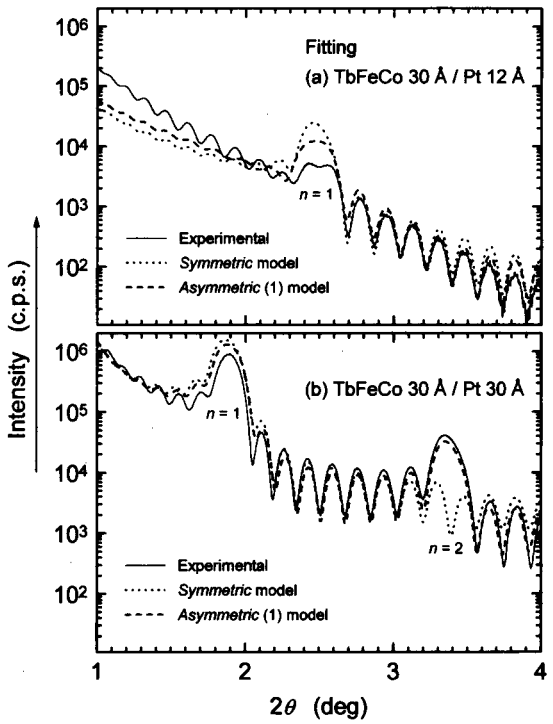

Fig. 7 Low angle X-ray diffraction and fitting results for the *Symmetric* and *Asymmetric* (1) cases in the (a) {TbFeCo 30 Å/Pt 12 Å} and (b) {TbFeCo 30 Å/Pt 30 Å} multilayers.

Pt layers is quite small compared with the M_a value. This figure shows the steady increase in δ with t_{Pt} up to about 12 Å, and then it seems to level off for the 50 Å TbFeCo case.

Although the total thickness of the interfacial alloy-like layer is obtained, one cannot determine the thickness of alloy-like layers at individual interfaces. In order to estimate it, low angle X-ray diffraction patterns were analyzed using the grazing incidence X-ray reflectivity technique (PHILIPS, WinGixa).[18),19)] Layer-thicknesses, including the overcoat layer, were used as parameters and determined so that the simulated pattern gives the best fit to the experimental data. The

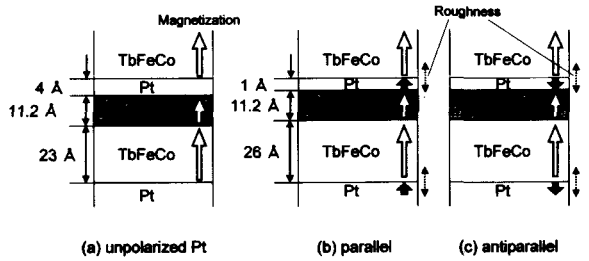

Fig. 8 Schematic *Asymmetric* models for the {TbFeCo 30 Å/Pt 12 Å} multilayer.

density and absorption coefficients were fixed as constants and the interface roughness was not taken into account in this fitting process. The simulation and fitting processes are described in Appendix. For simulation, a layered structure model was assumed where Fe–Pt alloy-like layers with a thickness δ in one period are present at interfaces (Pt/FePt/TbFeCo/FePt). The experimental data was analyzed for two cases. In the first case, there are two *symmetric* FePt layers in one period, *i.e.*, each FePt layer has the same thickness $\delta/2$ (*Symmetric* case). In the second, the FePt layers are present in an *asymmetric* fashion. Each FePt layer-thickness can be varied, while the total thickness δ is kept constant (*Asymmetric* case). This way, one can differentiate each FePt layer. Figure 7 shows low angle X-ray diffraction patterns for the (a) {TbFeCo 30 Å/Pt 12 Å} and (b) {TbFeCo 30 Å/Pt 30 Å} multilayers. The experimental data (——) are compared with the fitting results of the *Symmetric* (·····) and *Asymmetric* (1) (– – –) cases. In order to discuss quantitatively the fitting quality, a parameter called "fitting reliability" R' is used here. (The definition of R' is given in Appendix A.) The lower the value R', the better the fitting is.[20] For both the samples, it is of interest to find that the *Asymmetric* case is better for fitting, as shown in Fig. 7 and Table 1. Especially, this feature is manifested by the second order bilayer peak ($n=2$) of the (b) {TbFeCo 30 Å/Pt 30 Å} multilayer, where the *Asymmetric* (1) case can account for this peak while the *Symmetric* case cannot. This means that the Fe–Pt alloy-like layers are asymmetrically formed, as shown in Fig. 8(a). The simulation and fitting were also examined for the reversed structure, where the Fe–Pt alloy-like layer is formed on top of Pt, instead of TbFeCo. However, the fitting is worse than the previous one (see (2) *Reversed* case in Table 1). Therefore, it is concluded that the Fe–Pt alloy-like interface is formed on top of a TbFeCo layer, but not on a Pt layer. It seems that Tb, Fe, and Co atoms hardly diffuse into a Pt layer, keeping the interface sharp. On the other hand, Pt atoms may diffuse into an amorphous TbFeCo layer, consequently forming an Fe–Pt alloy-like interface.

In order for the whole experimental data to be consistent, it is important to explain the magneto-optical spectra based on the *Asymmetric* (1) model obtained

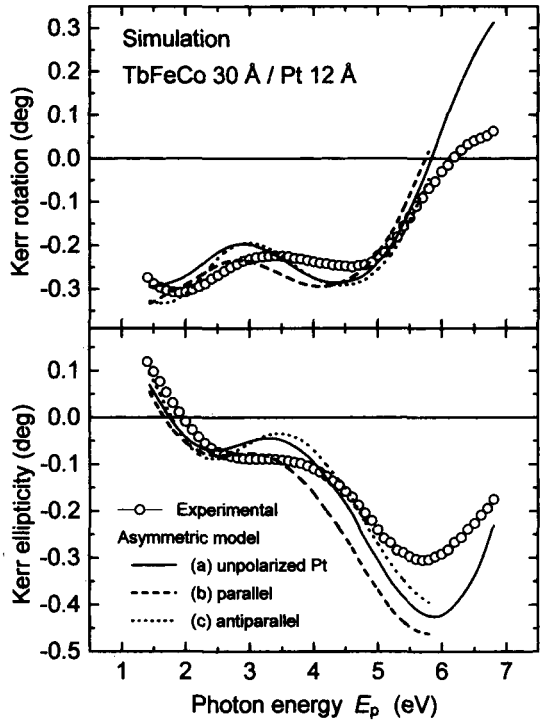

Fig. 9 Simulation of Kerr spectra for the *Asymmetric* models in the {TbFeCo 30 Å/Pt 12 Å} multilayer.

above. As a representative, Kerr spectra for the {TbFeCo 30 Å/Pt 12 Å} multilayer were simulated and compared with the experiment. A disordered fcc $Fe_{50}Pt_{50}$ alloy[21] was assumed as the Fe–Pt alloy-like layer in the model. The calculation procedure of Kerr spectra is as follows: 1) The Kerr rotation θ_K and ellipticity η_K and the optical constants n, k were experimentally measured as a function of photon energy for films of TbFeCo and disordered fcc $Fe_{50}Pt_{50}$ with thickness optically thick enough for accurate measurements. However, the optical constants of bulk Pt[22] were used for the case of unpolarized Pt. 2) The diagonal and off-diagonal dielectric elements, ε_{xx} and ε_{xy} are calculated using measured θ_K, η_K, n, and k. 3) Kerr spectra are calculated using the MULTILAYER computer program by Mansuripur.[23] Each layer of a multilayer-structure is identified by its thickness and dielectric tensor. In Fig. 9, Kerr spectra are compared between the experimental data (empty circles) and the simulation of the *Asymmetric* (1) model with *unpolarized* Pt (——). The overall spectral feature of the experimental data can reasonably be explained by the *Asymmetric* (1) model with *unpolarized* Pt. As previously reported in refs. 8–10, the interfacial Fe–Pt alloy-like is the essential for the enhancement in magneto-optical effect at high photon energies.

Further analyses of magneto-optical spectra were carried out. First, a roughness of the interface between Pt and TbFeCo was considered, while the interface of Fe–Pt alloy-like has no roughness. Simulation and

fitting for low angle X-ray diffraction patterns were carried out. The result is shown in Table 1 ((3) *Roughness* model). It is found that the better fitting ($R'=2.4$) is obtained by taking into account the roughness ($\sigma_j=$ 11 Å), as compared with the case where no roughness is considered ($R'=6.9$). Next, when the roughness is present, magnetic polarization of Pt atoms may occur. It was suggested that the transition between the *parallel* and *antiparallel* magnetic coupling may occur between FePt layer and Pt first monolayer in FePt/Pt multilayers.[24] In the present study, in order to shed light on this issue, hypothetical Pt layers with polarization *parallel* (ferromagnetic) or *antiparallel* (antiferromagnetic) to the FePt alloy layer were taken into account in the *Roughness* model (see Figs. 8(b) and (c)). The ε_{xy} data by Sato *et al.*[24] were used for the *parallel* polarization of Pt and the reversed ε_{xy} was applied to the *antiparallel* case in the calculation. The simulated Kerr spectra are compared in Fig. 9. In the *antiparallel* case (·····), the peak shifts toward higher energies compared to the *parallel* case (– – –), though it is not clear which is better to account for the observed results. A further detailed analysis may lead to better understanding of the role of Pt polarization.

5. Conclusions

The magnetic and magneto-optical properties of TbFeCo/Pt multilayer films are systematically studied. The results may be summarized as follows:

i) The saturation magnetization drastically increases with Pt thickness.
ii) The magneto-optical polar Kerr effect is significantly enhanced in ultraviolet photon energies.
iii) The low angle X-ray diffraction analysis reveals that the interfacial Fe–Pt alloy-like layers are asymmetrically formed only on the TbFeCo layer.
iv) This possibility is supported by simulation of magneto-optical spectra. Better fit is obtained by taking into account the spin-polarization of the Pt layer.

As a conclusion, the magnetic and magneto-optical properties can be reasonably well explained by taking into account asymmetric Fe–Pt alloy-like layers formed at the interfaces.

Appendix

The theoretical expression for the shape of a low angle X-ray diffraction pattern for multilayers having smooth boundary interfaces is considered as follows[18),19]: The thickness of each layer j ($j\leqq N$) is denoted by d_j. The reflectivity coefficient $R_{j,j+1}$ is given as a recursion formula:

$$R_{j,j+1}=\frac{R_{j+1,j+2}+F_{j,j+1}}{R_{j+1,j+2}F_{j,j+1}+1}\cdot a_j^4. \tag{2}$$

Here

$$F_{j,j+1}=\frac{g_j-g_{j+1}}{g_j+g_{j+1}},$$

$$a_j=\exp(-i\pi g_j d_j/\lambda),$$

where

$$g_j=\sqrt{n_j^2-\cos^2\theta},$$

λ is the wavelength, n_j is the refractive index of layer j, and θ is the angle of incidence. One solves Eq. (2) by starting at the substrate, layer N, and noting that $R_{N,N+1}=0$, since the thickness of the substrate is infinitely large. One also notes that a_1 is unity. Then, the ratio of the reflected to incident intensity I/I_0 is obtained by:

$$|R_{1,2}|^2=I/I_0. \tag{3}$$

For rough interfaces, the above formulas are no longer exact. To apply the Névot–Croce formulas[25] is a method to incorporate roughness. They assume that interface heights have a gaussian distribution. In the above recursion formulas, the Fresnel coefficient for reflection $F_{j,j+1}$ is multiplied by a factor S_j, expressed as:

$$S_j=\exp[-2(2\pi\sigma_j/\lambda)^2 g_j g_{j+1}], \tag{4}$$

which is a function of the root-mean-square deviation σ_j of the interface atoms from the perfectly smooth situation.

The following factor is employed to evaluate the fitting reliability.[20]

$$R'(\%)=\sqrt{\chi^2/\sum_{i=1}^{N_p}\{\log(I_{\exp}(\theta_i))\}^2}\times 100. \tag{6}$$

where χ^2 is defined as:

$$\chi^2=\sum_{i=1}^{N_p}\{\log(I_{\exp}(\theta_i))\}^2$$

Here $I_{\exp}$ and I_{cal} are measured and calculated intensities, respectively, and N_p is number of data points.

Acknowledgments The present work has been partially supported by the Original Industrial Technology R & D Promotion Program from the New Energy and Industrial Technology Development Organization (NEDO) of Japan (#8C-039-1), the Grant-in-Aid for International Scientific Research (Joint Research #09044186) from the Ministry of Education, Science, Sports, and Culture, and the Grant-in-Aid for Academic Frontier from the Ministry of Education, Science, Sports, and Culture (1999–2000).

References

1) P. F. Carcia: *J. Appl. Phys.*, **63**, 5066 (1988).
2) W. B. Zeper, F. J. A. M. Greidanus, P. F. Carcia, and C. R. Fincher: *J. Appl. Phys.*, **65**, 4971 (1989).
3) S. Hashimoto, Y. Ochiai, and K. Aso: *J. Appl. Phys.*, **67**, 2136 (1990).
4) K. Sato, H. Hongu, H. Ikekame, J. Watanabe, K. Tsuzukiyama, Y. Togami, M. Fujisawa, and T. Fukazawa: *Jpn. J. Appl. Phys.*, **31**, 3603 (1992).
5) H. Awano, T. Niihara, and M. Ojima: *J. Magn. Magn. Mat.*,

126, 550 (1993).
6) Y. Itoh, W. P. Van Drent, M. Birukawa, and T. Suzuki: *J. Magn. Soc. Jpn.*, **22** (Suppl. No. S2), 205 (1998).
7) Y. Itoh, W. P. Van Drent, and T. Suzuki: *J. Appl. Phys.*, **83**, 6753 (1998).
8) Y. Itoh, J. Weissenrieder, and T. Suzuki: *J. Magn. Soc. Jpn.*, **23**, 1081 (1999).
9) Y. Itoh, G. N. Phillips, T. Suzuki, and J. Weissenrieder: *J. Magn. Soc. Jpn.*, **23** (Suppl. No. S1), 55 (1999).
10) Y. Itoh and T. Suzuki: *IEEE Trans. Magn.*, **35**, 3121 (1999).
11) Y. Itoh and T. Suzuki: *J. Appl. Phys.*, **87**, 6902 (2000).
12) W. P. Van Drent and T. Suzuki: *J. Magn. Magn. Mat.*, **175**, 53 (1997).
13) Y. Hamajima, W. P. Van Drent, M. Matsuo, Y. Itoh, T. Kondo, A. Ishita, and T. Suzuki: *J. Magn. Soc. Jpn.*, **23**, 795 (1999).
14) G. H. O. Daalderop, P. J. Kelly, and M. F. H. Schuurmans: *Phys. Rev. B*, **44**, 12054 (1991).
15) T. Sugimoto, T. Katayama, Y. Suzuki, T. Koide, T. Sidara, M. Yuri, A. Itoh, and K. Kawanishi: *Phys. Rev. B*, **48**, 16432 (1993).
16) P. M. Oppeneer: *J. Magn. Magn. Mat.*, **188**, 275 (1998).
17) T. Katayama, T. Sugimoto, Y. Suzuki, M. Hashimoto, P. de Haan, and J. C. Lodder: *J. Magn. Magn. Mat.*, **104–107**, 1002 (1992).
18) L. G. Parratt: *Phys. Rev.*, **95**, 359 (1954).
19) D. K. G. de Boer: *Phys. Rev. B*, **44**, 498 (1991).
20) K. Usami and H. Suzuki: *J. Magn. Soc. Jpn.*, **18**, 38 (1994).
21) H. Kanazawa, T. Suzuki, Y. Itoh, and J. Osterman: *J. Magn. Soc. Jpn.*, **23** (Suppl. No. S1), 51 (1999).
22) *CRC Handbook of Chemistry and Physics*, ed. by D. R. Lide and H. P. R. Frederikse (CRC Press, Boca Raton, 1997), Chap. 12.
23) M. Mansuripur: *J. Appl. Phys.*, **67**, 6466 (1990).
24) K. Sato, Y. Tosaka, H. Ikekame, M. Watanabe, K. Takanashi, and H. Fujimori: *J. Magn. Magn. Mat.*, **148**, 206 (1995).
25) L. Névot and P. Croce: *Rev. Phys. Appl.*, **15**, 761 (1980).

Received July 12, 2000; Accepted August 25, 2000